



Soot formation from a distillation cut of a Fischer–Tropsch diesel fuel: A shock tube study

Olivier Mathieu^{a,1}, Nabiha Chaumeix^{b,*}, Claude-Etienne Paillard^b

^a Total Raffinage Marketing, La Defense, France

^b Institut de Combustion, Aérothermique, Réactivité et Environnement, CNRS Orléans, 1c, avenue de la recherche scientifique, 45071 Orléans Cedex 2, France

ARTICLE INFO

Article history:

Received 5 October 2011

Received in revised form 11 January 2012

Accepted 24 January 2012

Available online 3 March 2012

Keywords:

Soot formation

Fischer–Tropsch

Shock tube

ABSTRACT

The kinetics of soot formation from Fischer–Tropsch (FT) fuels was studied in a heated shock tube under homogeneous conditions. Soot induction delay time and soot yield were measured between 10 and 17 atm using a distillation cut at 403 K of a Fischer–Tropsch fuel diesel. Two fuel concentrations were investigated in pyrolysis: 0.2% and 0.4% FT in Ar. Equivalence ratios (Φ) = 18 and 5 were also investigated for the highest fuel concentration. During this study, a second growth of the soot volume fraction profile was observed with the highest fuel concentration in pyrolysis and at Φ = 18. It was shown that this second growth appears only at temperatures higher than the temperature at which the soot yield is maximum. Under the conditions investigated, the soot induction delay time was found not to be very sensitive to the fuel concentration. A careful analysis of the soot volume fraction profiles showed that this finding was linked to the measurement method usually adopted. Nevertheless, this method was found adequate for a systematic comparison between different fuels or for an investigation of the oxygen concentration effects. The addition of oxygen to the mixture promotes soot formation in its early stages by decreasing the soot induction delay time. A shift of the soot yield curve toward lower temperatures was also observed. Moreover, oxygen addition reduces the amount of soot produced. This reduction is proportional to the O₂ concentration. Comparisons with literature data showed that a Fischer–Tropsch fuel primarily composed of *n*-paraffins can be correctly represented by an *n*-paraffin with a molecular size comparable to the average molecular size of the Fischer–Tropsch fuel. The maximum soot yield of the Fischer–Tropsch distillation cut studied was not significantly different from that of a diesel fuel surrogate previously studied (Mathieu et al., Combust. Flame 156 (2009) 1576–1586).

© 2012 The Combustion Institute. Published by Elsevier Inc. All rights reserved.

1. Introduction

Due to the adverse health effects of soot particles [1], legislation concerning their emission has become more and more stringent over recent years in most developed countries. To reduce soot particle emissions from vehicles and meet the requirements of the legislation, several methods, often complementary, can be employed. One can mention improvements of the engine technology (e.g. fuel injection system), changes to the after-treatment system, and fuel formulation. Among these methods, fuel formulation presents the advantage of being engine-technology-independent and thus, directly applicable to the entire fleet of existing vehicles. Fuel formulation also allows a decrease of the regeneration frequency of the after-treatment system and of the associated fuel consumption penalty.

* Corresponding author. Fax: +33 238 696 004.

E-mail address: chaumeix@cnrs-orleans.fr (N. Chaumeix).

¹ Current address: Department of Mechanical Engineering, Texas A&M University, College Station, TX, USA.

The Fischer–Tropsch (FT) process has been used for decades to produce synthetic diesel fuels, almost exclusively composed of *n*- and *iso*-paraffins [2], from any carbonaceous feedstock (natural gas [2], coal [3], or biomass [4]). The literature generally reports an ability of Fischer–Tropsch fuels, either used pure or blended with conventional fuels, to reduce particle emissions from light- and heavy-duty diesel vehicles [5]. However, probably because of the use of different engines, operated at different running conditions, the amplitude of these reductions (if any) can vary significantly between any two studies [5]. Sometimes an increase in the smoke quantity can even be observed with modern diesel engine technology [6] when the injection timing is not adjusted. These observations make obvious the need for a study of FT fuels in a well-controlled environment, such as a shock tube, to assess their intrinsic sooting propensity without the complications of the physical processes present in engines.

Soot formation from FT fuels was investigated in a shock tube using a direct liquid injection technique that allows the study of fuels under conditions comparable to those encountered in engines [7]. Unfortunately, the use of liquid spray introduces heterogeneities

Nomenclature

[C]	carbon concentration in atom cm^{-3}	T_{opt}	optimal temperature of soot formation
f_v	soot volume fraction	t_{obs}	practical observation time
$f_{v\text{max}}$	maximum value attained by the f_v signal	Y	soot yield
N_{av}	Avogadro's number, 6.023×10^{23} molecules/mole	Y_{max}	maximum soot yield
P_5	pressure behind the reflected shock wave	ρ	soot density, 1.86 g/cm^{-3}
Q	integration constant	τ_{ind}	soot induction delay time
RSW	reflected shock wave	Φ	equivalence ratio
T_5	temperature behind the reflected shock-wave		

in fuel concentration and equivalence ratio (Φ), which prevent accurate determination of kinetic data behind the reflected shock waves (RSW). As a result, the kinetic data determined under these conditions are not easily usable and one can conclude that the determination of soot kinetics data (induction delay time and soot yield) obtained under homogeneous and well-defined conditions is still needed for FT fuels.

In addition, it is worth mentioning that there are relatively few shock-tube data available for alkanes larger than C4 in the literature. Indeed, although the *n*-alkanes family has been relatively well covered (*n*-hexane [8], *n*-heptane [9–12], *n*-decane [13], and *n*-hexadecane [14]), data for *iso*-alkanes are still scarce (*iso*-octane (2,2,4-trimethylpentane) [15] and *iso*-cetane (2,2,4,4,6,8,8-heptamethylnonane) [16]), with all the studies concerning paraffins larger than C7 coming from our group. To our knowledge, there are no data available for mixtures of *n*- and *iso*-alkanes.

The aim of this study is to determine these kinetic data for soot formation under homogeneous conditions for a FT fuel constituted of normal and *iso*-paraffins. Another objective is to provide evidence of the carbon concentration dependence of the second growth stage of the soot volume fraction (f_v), a phenomenon that was recently studied in a shock tube [16].

Due to the limitations of the heating system of the shock-tube setup (limited to 423 K), the soot formation process was investigated using a distillation cut at 403 K of a FT diesel fuel. This cut was studied at two concentrations (0.2% and 0.4% (molar)) in pyrolysis and at $\Phi = 18$ and 5. This range of equivalence ratios covers the wide range of conditions that can be found during the combustion cycle of a diesel engine. The equivalence ratio of 5 was more particularly selected as it corresponds to the lower limit under which it becomes difficult to study with accuracy the kinetics of soot formation in our conditions. To assess the soot propensity of

this FT distillation cut, results are compared with those from a diesel surrogate [16]. The average molecular weight of this FT distillation cut, which is close to the molecular weight of *n*-decane, also makes these data valuable to assess the soot tendency for the jet fuels boiling range.

2. Experimental setup

Experiments were conducted in a heated stainless steel shock tube (driven section 5.15 m long, 52 mm i.d., driver section 2 m long, 114 mm i.d.) (Fig. 1). The last part of the driven section was equipped with four piezoelectric shock detectors (Chimie Metal, Model A25L05B). These shock detectors have a diameter of 2 mm with a sensitive surface area of 0.75 mm^2 and a rise time of $0.4 \mu\text{s}$. The very small surface area coupled with a short rise time allows precise determination of the shock wave passage and, consequently, more accurate evaluation of the temperature and pressure behind the reflected shock wave (reflected shock pressure, P_5 , and temperature, T_5 , were calculated using the classical procedure [17]). On the other hand, these transducers are very sensitive to heat transfer and a continuous increase of the signal is observed after the jump due to the passage of the shock waves (Fig. 2). This increase in the signal is due to the limited increase of the gas temperature in the boundary layer, which is sufficient to induce a signal drift that would wrongly lead to the conclusion that the pressure (and hence the temperature) increases strongly immediately behind the reflected shock wave. After this continuous rise in the signal, the end of the observation time is given by the decrease of the pressure signal associated with the arrival of the rarefaction waves. Recently, a Kistler pressure transducer (603B) has been installed at the endwall of the shock tube. A comparison of

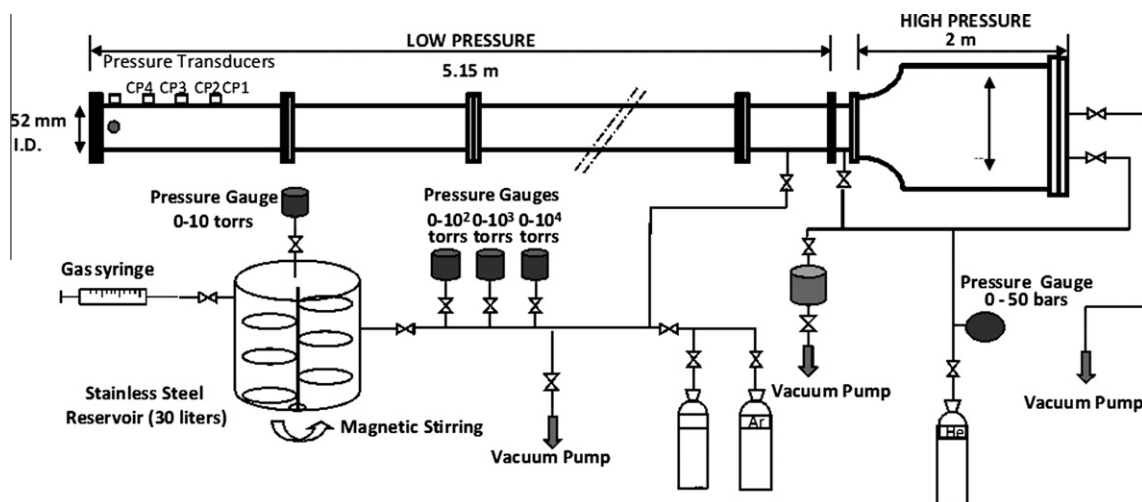


Fig. 1. Layout of the experimental setup used during this study.

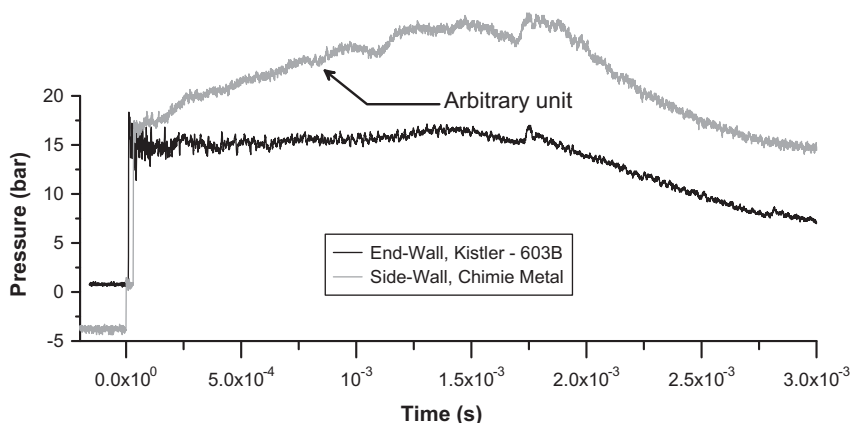


Fig. 2. Comparison between the signals delivered by the Kistler (603B) pressure transducer (black line) and the Chimie Metal shock detector (gray line, in arbitrary units).

the signal delivered by the two transducers (Chimie Metal on the sidewall location and Kistler on the endwall) during a run with Ar is visible in Fig. 2. As seen, the assumption of constant pressure and temperature behind the reflected shock wave is verified for our highly diluted mixtures.

Sidewall shock detectors are equally spaced at 150 mm and mounted flush with the inner surface. The last transducer was located 10 mm before the shock-tube end wall. Two fused silica windows (9-mm optical diameter, 6-mm thickness) were mounted in the same plane as the last transducer. A slight attenuation (around 1%) of the shock wave was recorded over the measurement section. To minimize the influence of this attenuation on P_5 and T_5 determination, the speed of the shock wave was measured using the last two transducers. A high-frequency digitizing oscilloscope recorded the He–Ne laser light attenuation (632.8 nm) detected by a photomultiplier (Hamamatsu R928) equipped with an interference filter (Melles Griot, 633 ± 2 nm). At this wavelength, the light extinction is primarily due to the soot particles, although the effect of the large compounds containing more than six aromatic rings was reported [18]. To avoid multiple reflections of light, the measurement section was blackened by anodic oxidation over a length of 70 cm. The measurements are based on the Beer–Lambert law

(see [16] for more details) and the soot volume fraction (f_v) was calculated using the soot refractive index provided by Lee and Tien [19] with a soot density (ρ) of 1.86 g cm^{-3} . A recent and careful measurement of the soot refractive index has been performed by Williams et al. [20] at a wavelength (635 nm) very close to the wavelength used in this study. The refractive index used was, however, selected for convenient comparison with literature results [13–16]. It is worth mentioning that depending on the value of the refractive index selected, the calculated soot yield can differ by almost a factor of 4 [13].

The FT distillation cut used was composed only of paraffins (57.2% *n*-paraffins, 42.8% *iso*-paraffins, in molar percentage). The molecular size distribution (in terms of carbon number) is known (Table 1) but the detailed composition of *iso*-paraffin isomers was not available.

The lack of this information was problematic for the accurate calculation of temperature and pressure behind RSW, since the thermodynamic data for the mixture components are required. To overcome this difficulty, we considered the *iso*-paraffins as *n*-paraffins. This approximated composition is responsible for an error in the P_5 and T_5 determinations. This error was assessed by calculating and comparing P_5 and T_5 over the whole range of conditions investigated for a mixture of 0.4% *n*-octane in argon and for a mixture composed of *n*-octane and *iso*-octane in FT's proportion (0.23% and 0.17%, respectively). Calculated results for the two mixtures show differences between 0.17% and 0.2% in temperature and between 0.02% and 0.05% in pressure. These errors are very small compared to the experimental error in T_5 and P_5 determinations (estimated around $\pm 1.5\%$). Hence, we considered these approximations negligible for the determination of the reflected shock parameters. Thermodynamic properties for *n*-paraffins were taken from the literature [21] or calculated ($n\text{-C}_{13}$ to $n\text{-C}_{15}$) using THERM software [22] that uses group additivity rules developed by Benson [23].

The reactive mixtures were prepared manometrically. The liquid fuel was introduced into the mixing tank (30 l) through a septum using a gas syringe and was allowed for vaporizing and mixing using a magnetic stirrer for 15 min. Tests were conducted to determine the volume of fuel for which all the fuel will evaporate.

Table 1
Molar composition for the distillation cut at 403 K of a FT diesel fuel.

Number of carbons	Molar percentage	
	<i>n</i> -Paraffin	<i>iso</i> -Paraffin
7	0.48	0.35
8	2.19	1.63
9	8.51	6.37
10	10.79	8.07
11	10.14	7.57
12	9.52	7.12
13	8.54	6.39
14	5.55	4.16
15	1.49	1.12
Total	57.22	42.78

Table 2
Summary of the experimental conditions for diluted mixtures in Ar.

Fischer–Tropsch ($\text{C}_{11.23}\text{H}_{24.46}$) (%)	T_5 (K)	P_5 (MPa)	[Carbon] ₅ (atoms/cm ³)	Φ	O ₂ % (vol.) in Ar
0.4	1675–2540	1.24–1.71	$(1.83\text{--}2.76) \times 10^{+18}$	∞	0
	1630–2325	1.51–1.65	$(2.11\text{--}2.50) \times 10^{+18}$	18	0.42
	1525–1920	1.05–1.48	$(2.17\text{--}2.49) \times 10^{+18}$	5	1.33
0.2	1500–2225	1.15–1.65	$(1.15\text{--}1.38) \times 10^{+18}$	∞	0

The amount of fuel used to prepare mixtures was kept well below this value. To prevent slow degradation of the fuel in the heated stainless steel tank over time, a new mixture was prepared prior to each run. The whole setup was kept at a temperature of 405 ± 2 K and the shock tube was carefully cleaned after each run. Investigated conditions are summarized in Table 2. The lowest value of the range of temperatures investigated corresponds to the minimum temperature at which soot formation can be detected, whereas the highest value corresponds to the temperature at which the soot yield decrease to a value near zero. Note that a second regime of soot formation can be found for higher temperatures, above 2500 K [24,25]. This very-high-temperature regime was not studied, as it was not of practical relevance for diesel engines.

3. Results

3.1. Soot volume fraction profile (f_v)

The evolution of the soot volume fraction versus time is plotted for some FT/argon pyrolysis cases in Fig. 3a and b. At a reflected temperature of 1914 ± 5 K (Fig. 3a), one can see two soot volume fraction profiles corresponding to two different initial carbon atom concentrations: 1.24×10^{18} and 2.45×10^{18} C atoms cm^{-3} . For the same initial carbon atom concentration, soot volume fractions at a higher reflected shock temperature, 2049 ± 9 K, are reported (Fig. 3b). For a reflected shock temperature of around 1914 K (Fig. 2a), f_v increases with time following a sigmoid profile after a given delay between the arrival of the RSW and the beginning of the soot detection. This delay corresponds to the soot induction delay time and will be discussed in more detail later. After this delay, the soot volume fraction profile undergoes a period of growth until f_v reaches a maximum value ($f_{v\max}$). At around 2040 K (Fig. 3b), a similar soot volume fraction profile can be observed for the low carbon concentration case, whereas a two-step growth profile is clearly visible for the higher carbon concentration. During our experiments, this second growth process was observed for the highest fuel concentration and for temperatures above 1920 K under pyrolysis conditions.

This two-“step” growth is, however, observed not only for the pyrolysis case but also when oxygen is added to the mixture, as

can be seen in Fig. 4. At an initial temperature of around 1855 K (Fig. 4a), an addition of small amount of oxygen ($\phi = 18$) induces a rapid increase of the soot volume fraction compared to the pyrolysis case and leads to the same amount of soot at the end of the first growth process. Then, at around 1.5 ms, a second growth occurs at a rate similar to that of the pyrolysis condition, leading to a final soot load lower than for the pyrolysis condition run. For a higher temperature of around 2050 K, as shown in Fig. 4b, similar observations can be made. The soot appearance is detected earlier when oxygen is present, leading to a period of faster growth. The second step, which is observed with or without oxygen, occurs at the same time in both cases and with similar rates. It can be seen that the presence of oxygen does not significantly modify the contribution of the second growth to $f_{v\max}$ (around 30% of $f_{v\max}$ in pyrolysis and around 25% at $\phi = 18$). At around 2050 K, unlike around 1855 K, the presence of oxygen drastically reduces the soot volume fraction during these two growth steps. The double growth of f_v was not observed at $\phi = 5$.

3.2. Soot induction delay time

For comparison with literature data purpose, the soot induction delay time (τ_{ind}) was defined using the classical method [10–16]. In this method, τ_{ind} corresponds to the time interval between the moment at which the fuel mixture is heated by the RSW and the moment at which soot particles are detected (defined as the intersection of the inflectional tangent with the time axis), as visible in Fig. 5. The error associated with the measurement of this parameter is between 10% and 25% [16]. In some cases, however, as visible in Fig. 5, this method can lead to wrong interpretation of the data. In the examples given in Fig. 5, this method led to induction delays of 950 and 1020 μs for the cases at 0.2 and 0.4% FT, respectively. However, the soot volume fraction at 950 μs is 1.45×10^{-8} at 0.2% FT and 3.6×10^{-8} at 0.4% FT. At 1020 μs , the soot volume fraction for 0.4% FT has already reached a value of 5.13×10^{-8} , which is more than three times higher than that for the 0.2% FT level at its corresponding induction delay time.

From these observations, it can be deduced that the classical technique for measuring the soot induction delay time, although valuable for literature data comparison for similar experimental conditions, does not seem to be adequate for a comparison

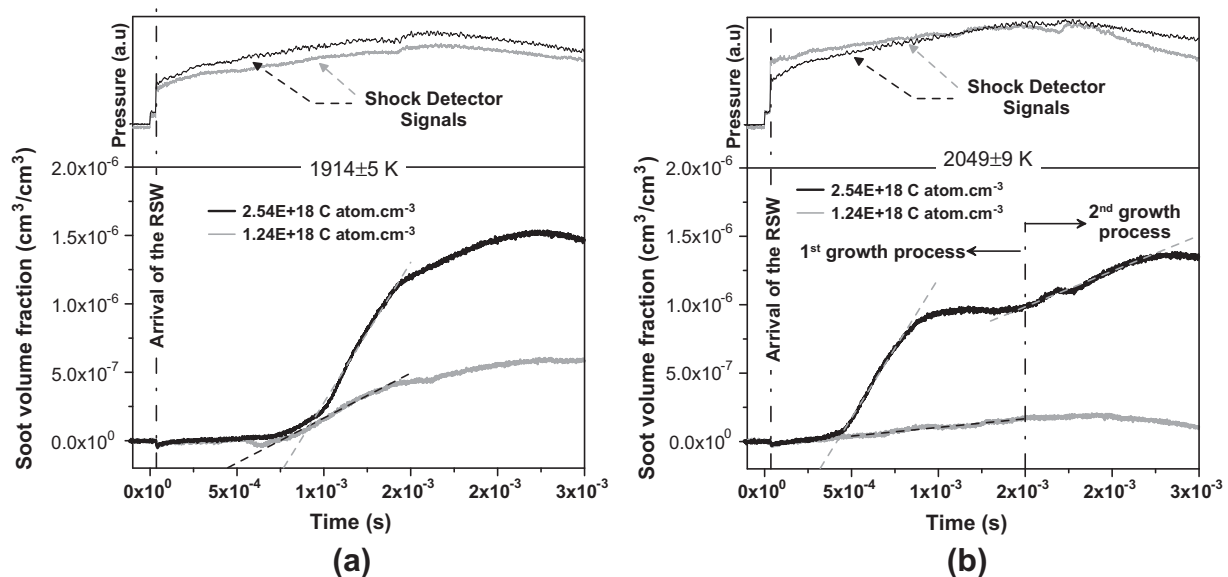


Fig. 3. Temporal evolution of the soot volume fraction for a cut of a FT fuel in pyrolysis at two different concentrations. (a) Black line: 1919 K, 1.44 MPa; gray line: 1909 K, 1.48 MPa. (b) Black line: 2049 K, 1.6 MPa; gray line: 2031 K, 1.51 MPa.

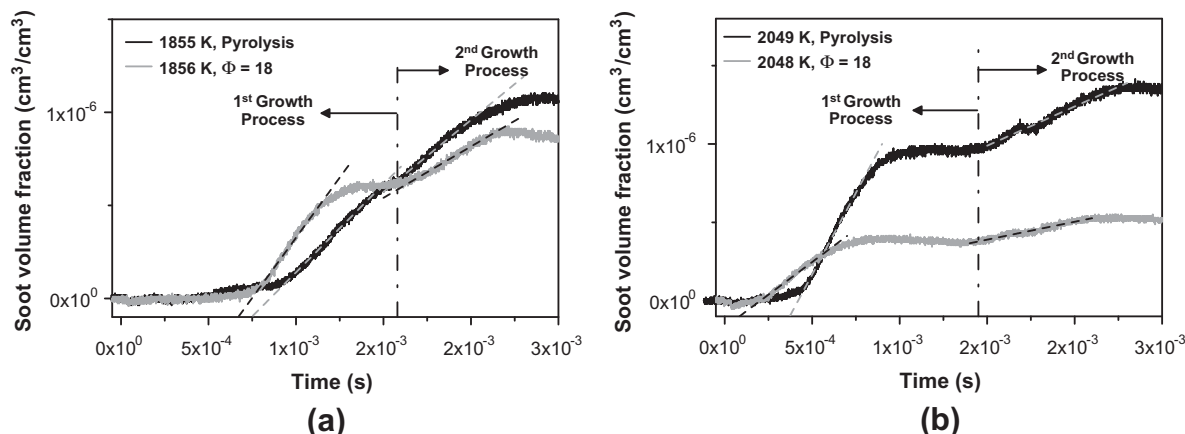


Fig. 4. Temporal evolution of the soot volume fraction for a cut of a Fischer–Tropsch fuel in pyrolysis and at $\Phi = 18$. (a) Black line: 1.37 MPa, 2.35×10^{18} C atom cm^{-3} ; gray line: 1.32 MPa, 2.30×10^{18} C atom cm^{-3} . (b) Black line: 1.60 MPa, 2.54×10^{18} C atom cm^{-3} ; gray line: 1.55 MPa, 2.38×10^{18} C atom cm^{-3} .

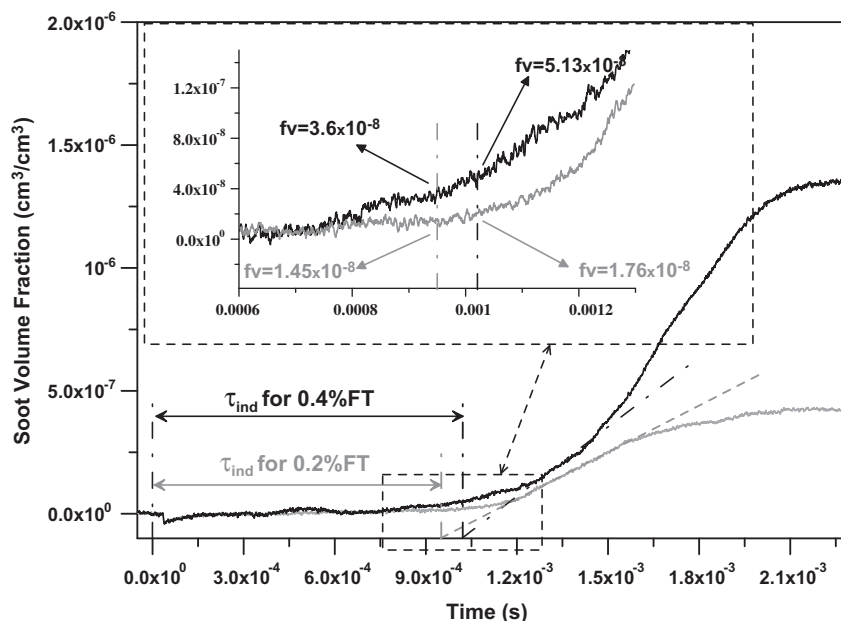


Fig. 5. Illustration of the classical measurement method of the soot induction delay time and its deficiency in representing the variation of the induction delay with the fuel concentration.

between results obtained at the two carbon concentration investigated during this study. This is confirmed, as is shown in Fig. 6, in which the evolution of τ_{ind} with $1/T_5$ with this classical method is plotted. Indeed, results in pyrolysis indicate that the FT concentration has no noticeable effect on the soot induction delay time: very similar values of τ_{ind} and activation energy (E_a) were measured. Careful observation of this Fig. 6 even shows that the induction delay times are, overall, slightly longer at 0.4% FT, which is not what is observed in Fig. 5.

Concerning the results obtained with oxygen at the highest fuel concentration, the classical method gives valuable results in terms of tendency. It is clearly visible in Fig. 6 that the oxygen concentration has a strong effect on the induction delay: at 1800 K, $\tau_{\text{ind}} = 1145 \mu\text{s}$ in pyrolysis, 865 μs at $\Phi = 18$, and 395 μs at $\Phi = 5$.

The activation energy was found to be independent of the oxygen concentration, as can be seen in Table 3:

At $\Phi = 5$, where the soot amount and the slope of the growth of the soot volume fraction profile are low compared to the other conditions, the method of measurement of the soot induction delay

time used creates a higher uncertainty (estimated around 25%), which can explain the relative scattering of the data and the slightly higher value of E_a . Over the range of conditions investigated, an average value of 162 kJ/mol for the activation energy can be derived, which is close to the average value determined for large alkanes [13,14,16].

3.3. Soot yield

Soot yield (Y) is defined as the ratio of carbon content present in soot to the initial carbon concentration. The initial carbon concentration, $[C]_{\text{initial}}$ (atoms cm^{-3}), behind RSW is easily deduced from the initial fuel concentration, while the concentration of carbon transformed to soot is deduced from the laser extinction signal using Graham's model [26]. This model allows the determination of the soot yield using the soot volume fraction directly:

$$Y (\%) = \frac{N_{\text{av}} \rho f_v}{12 [C]_{\text{initial}}} \times 100, \quad (1)$$

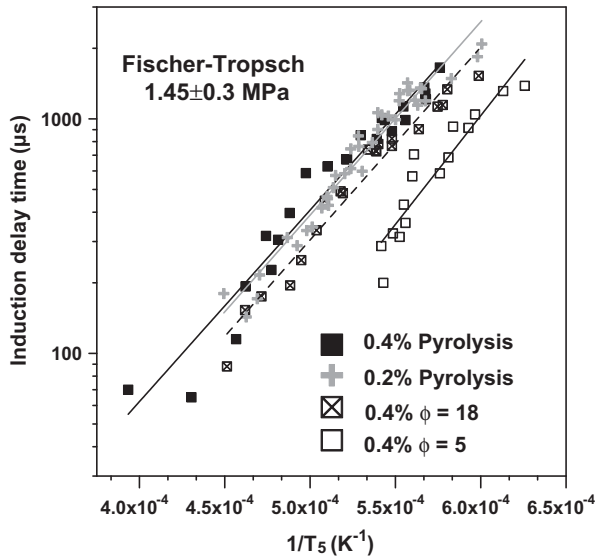


Fig. 6. Evolution of the soot induction delay with the temperature behind the RSW for a distillation cut at 403 K of a Fischer-Tropsch fuel at two carbon atom concentrations (0.2% and 0.4%) in pyrolysis and at equivalence ratios of 18 and 5 (for the 0.4% FT case).

Table 3

Kinetics parameters for the induction delay time deduced from Fig. 6 according to the equation $\tau_{\text{ind}}(s) = Ae^{(E_a/RT)}$.

Mixture	A	E_a (J mol ⁻¹)
0.4% FT, pyrolysis	33.71×10^3	156350 ± 8.500
0.2% FT, pyrolysis	29.37×10^3	157100 ± 8.500
0.4% FT, $\phi = 18$	23.60×10^3	157400 ± 8.500
0.4% FT, $\phi = 5$	2.80×10^3	177600 ± 36.500

where N_{av} is Avogadro's number. To calculate the soot yield, the value of f_v obtained at 2 ms was used. This time is equivalent to the observation time in the shock tube. In the present study, this time is also close – or corresponds – to the maximum value reached by the soot volume fraction signal (Fig. 3).

The evolution of the soot yield with the temperature for the different investigated conditions is visible in Fig. 7 where the evolution of the soot yield as a function of the temperature follows

Table 4

Values extracted from Fig. 7 using Eqs. (2) and (3).

Fischer-Tropsch (% mol. in Ar)	Equivalence ratio	Y_{max} (%) Eq. (2)	T_{opt} (K)	Q	Y_{max} (%) Eq. (3)
0.4	Pyrolysis	6.2	1955	104.85	–
	18	3.7	1870	75.60	3.9
	5	1.3	1705	166.30	1.8
0.2	Pyrolysis	4.6	1850	131.40	–

the classical bell shape. Values for the maximum soot yield (Y_{max}) and for the temperature at which Y_{max} occurs (T_{opt}) were extracted using the best fit (greatest coefficient of determination, R^2) of the equation proposed in [16,27],

$$Y = Y_{\text{max}} \cdot \exp \left(-Q \left[\frac{T_{\text{opt}} - T_5}{T_5} \right]^2 \right), \quad (2)$$

where Q is a correlation factor. The different parameters (Y_{max} , T_{opt} , and Q) derived by applying Eq. (2) to the results plotted in Fig. 7 are summarized in Table 4.

A comparison between the pyrolysis results, at fuel molar percentages of 0.2% and 0.4%, allows the study of the effect of carbon concentration (Fig. 7a). It can be seen that the maximum soot yield increases notably with the carbon concentration: $Y_{\text{max}} = 4.6\%$ and 6% at 0.2% and 0.4% FT, respectively. The increase in carbon concentration also has an impact on T_{opt} : T_{opt} is around 1850 K at 0.2% FT concentration and around 1920 K at 0.4% FT. The temperature at which the first soot particles were detected is also dependent on the carbon atom concentration. Indeed, soot particles were detected above 1600 K for 0.2% FT and only above 1700 K for the highest investigated concentration.

Figure 7b also shows that the effect of oxygen concentration on the soot yield is important: compared to pyrolysis, Y_{max} is decreased by around 37% at $\phi = 18$ ($Y_{\text{max}} = 3.8\%$) and by more than 75% at $\phi = 5$ ($Y_{\text{max}} = 1.4\%$). The presence of oxygen also shifts the temperature at which the first soot particles can be observed toward low temperatures: around 1600 K at $\phi = 18$ and 1500 K at $\phi = 5$.

4. Comparison with literature data

Pyrolysis results obtained during this study were compared with literature data for *iso*-paraffins (*iso*-octane [15] and *iso*-cetane [16]), for *n*-paraffins (*n*-decane [13] and *n*-hexadecane (or cetane)

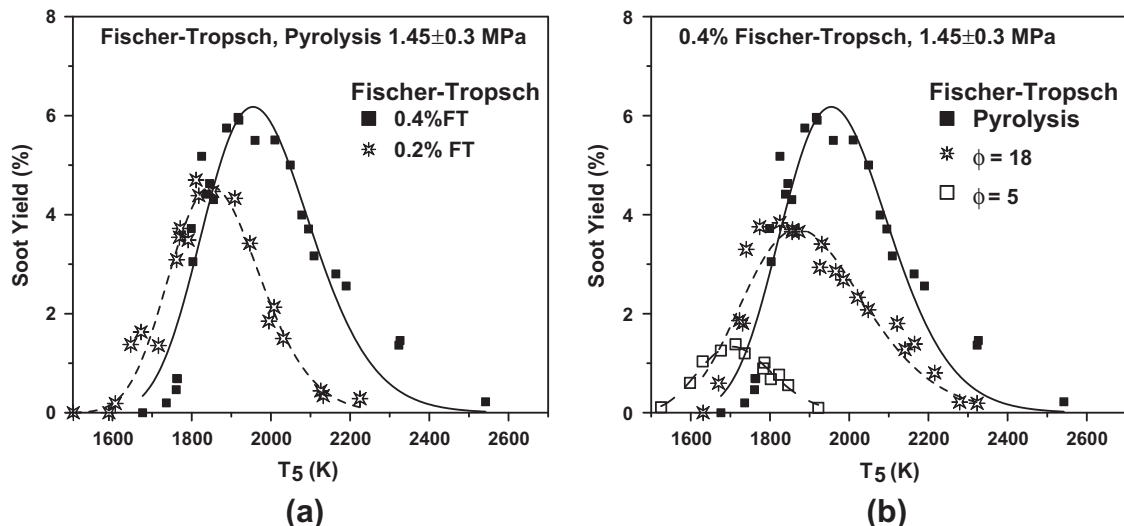


Fig. 7. Evolution of the soot yield with the temperature behind the RSW for a distillation cut at 403 K of a Fischer-Tropsch fuel (lines: best fit using Eq. (2)).

[14]), and for a diesel fuel surrogate [16]. This data was obtained using the same shock tube and under conditions similar to the present study. The comparison between paraffins and other classes of components (aromatics, naphthenes) was reported in former studies [14–16].

Figure 8 shows the results obtained for the soot induction delay time with the aforementioned paraffins. The induction delay times presented in Fig. 8 were measured using the classical method of determination (Fig. 5). It is visible from Fig. 8 that FT, along with *n*-decane, exhibits the longest induction delay times. Results obtained with cetane and *iso*-cetane show that τ_{ind} is comparable for *iso*- and *n*-paraffin isomers. This observation is confirmed in the present study by comparing FT and *n*-decane [13] results. Comparing *n*-decane to *n*-hexadecane and *iso*-octane to *iso*-cetane shows that the smaller the paraffin molecule is, the longer the induction delay time. From these observations, it can be concluded that results obtained with the FT ($\text{C}_{11.23}\text{H}_{24.46}$), which are close to those of *n*-decane, are in agreement with literature data. Activation energies of the aforementioned paraffins are equal to 175 ± 19 kJ/mol, except for the *iso*-octane (118 kJ/mol).

Comparison between FT and the diesel surrogate (39% propylcyclohexane/28% butyl-benzene/33% 2,2,4,4,6,8,8-heptamethylnonane, in mass proportion) shows that the FT has a lower soot tendency: τ_{ind} for the FT is between 2.7 (low temperatures) and 6 times (high temperatures) longer than τ_{ind} for the diesel surrogate.

Comparison of the evolution of the soot yield with T_5 for the FT, *n*-decane, *n*-hexadecane, *iso*-octane, and *iso*-cetane is visible in Fig. 9. It can be seen on this figure that for each type of paraffin (*n*- and *iso*-), at constant carbon concentration, the longer the molecule, the lower the soot yield. Comparison between *iso*- and *n*-paraffins indicates that *iso*-paraffins produce more soot under similar conditions. For the FT, as for the τ_{ind} , results are very similar to *n*-decane, except that the FT produced more soot than *n*-decane above 1920 K. This effect of the branching of paraffin molecule on soot formation has been investigated for hexane isomers [28] and the fact that few differences are visible between the soot yield curve of the FT and *n*-decane is probably due to the larger proportion of *n*-paraffins in the FT composition. It is also likely that the degree of branching of the FT's *iso*-paraffins is small, which is usually the case for FT fuels [29,30]. One of the main outcome of the present study is that a FT mainly composed of *n*-paraffin can be represented by *n*-paraffin of comparable size for applications where the boiling curve does not have to be considered (even if, in the present case, the FT cut would have been probably better

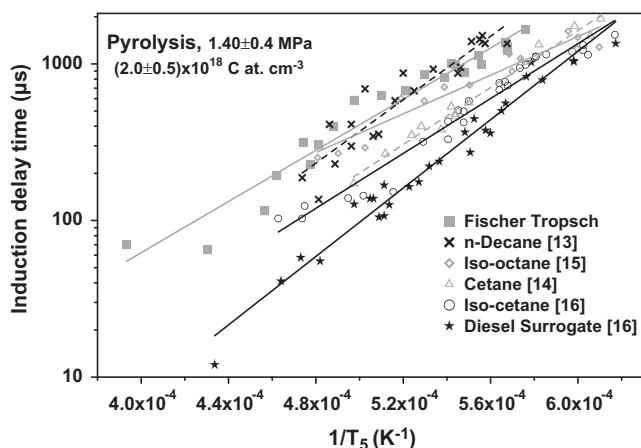


Fig. 8. Evolution of the soot induction delay with the temperature behind the RSW for a distillation cut at 403 K of a Fischer–Tropsch fuel, *n*-decane [13], cetane [14], *iso*-octane [15], *iso*-cetane [16], and a diesel surrogate [16].

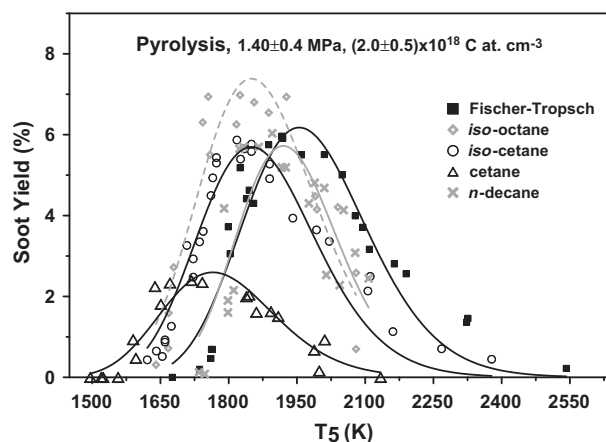


Fig. 9. Evolution of the soot yield with the temperature behind the RSW for a distillation cut at 403 K for a Fischer–Tropsch fuel, *n*-decane [13], cetane [14], *iso*-octane [15], and *iso*-cetane [16] (lines: best fit using Eq. (2)).

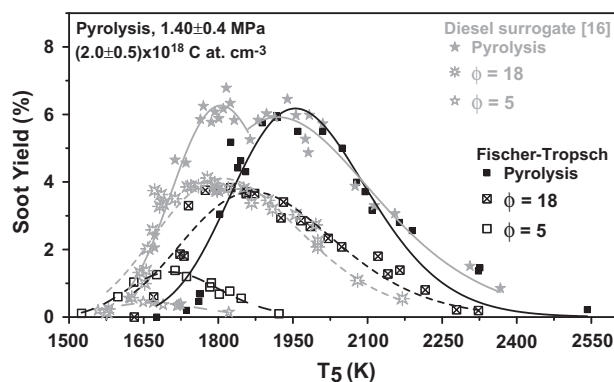


Fig. 10. Evolution of the soot yield with the temperature behind the RSW for a distillation cut at 403 K of a Fischer–Tropsch fuel and a diesel surrogate [16]. (Lines: best fit using Eq. (2). Note that Eq. (2) was applied on each peak for the diesel surrogate; see [16].)

represented by a 2- or 3-methyl-decane or a 2,3-dimethylnonane). In literature, a FT has already been represented by a single paraffin [31]. This former assessment, however, was not validated by any experimental or numerical investigation.

Figure 10 shows the comparison of soot yield between the FT and the diesel surrogate (39% *n*-propylcyclohexane, 28% *n*-butylbenzene, and 33% *iso*-cetane, in mass), in pyrolysis and at $\Phi = 18$ and 5. It can be seen that the FT, while composed of several paraffins, exhibits only one maximum soot yield. Thus, the two maxima observed on the soot yield curve of the diesel surrogate can be associated with its composition, meaning that there are no synergistic effects between different natures of hydrocarbon in that particular case. Overall, the maximum soot yield of the FT is comparable to, yet lower than, the maximum soot yield of the surrogate in pyrolysis and at $\Phi = 18$. Under both conditions, the diesel surrogate starts producing soot at slightly lower temperature. In pyrolysis, when considering the temperature range where soot particles are produced, it can be deduced that the surrogate has a higher soot tendency than the FT. However, the FT produces more soot than the diesel surrogate at $\Phi = 5$.

5. Discussion

The investigation of the soot formation process from a distillation cut at 403 K of a FT diesel fuel demonstrated the presence of

a second growth of the soot volume fraction for the higher carbon concentration in pyrolysis and at $\Phi = 18$. This second growth of f_v was observed in the literature with various hydrocarbons and mixture of hydrocarbons [16,11] and for hydrogen-free compounds [32]. The carbon-concentration dependence of this phenomenon was observed previously in [16], where toluene pyrolysis results were compared between two studies [14,27]. The theory of the chemical origin of this second growth of f_v postulated in [16] is supported by the following facts observed during this study: (i) the temperature at which this second growth appears is sensitive to the oxygen concentration and (ii) the effect of oxygen concentration on the amplitude of this second growth depends on the structure of the initial fuel (as can be seen, for example, by comparing results from Fig. 4 with results from *n*-butyl-benzene in [16]). At very high temperatures (above 2300–2500 K), a second regime of soot formation was reported in the literature with shock tube experiments [24,25]. This secondary regime was attributed to the C2 radical contributions [33] and it has been found in [16] that it is not possible to clearly link the double growth of the soot volume fraction observed in our experiments with this second regime occurring at higher temperatures.

It is also worth noting that the maximum value reached by the double growth of f_v is generally observed a few hundreds of microseconds after the observation time (t_{obs}), which is typically around 2 ms in our experiments. The comparison of soot volume fraction profiles with and without extension of the observation time was made in a former study with propylcyclohexane [16]. It was shown that, with the present shock tube configuration, the second growth of f_v is not influenced by the expansion wave during the first hundreds of microseconds after t_{obs} , where the change in density is small. A similar conclusion was reached from emission and extinction profiles by Agofaonov et al. [34] during the soot formation process from propane with or without FeCO_3 . Based on these observations, it is assumed that a qualitative description of the second growth of the soot volume fraction can be conducted until this second growth reaches its maximum value (between 2 and 2.5 ms, typically). To date, there is still no clear explanation or satisfactory theory of this second growth phenomenon. A thorough experimental study on the effects of the carbon concentration, the test time, the temperature evolution during the test time, the gas phase composition surrounding the soot particles, the adsorbed phase composition, and the soot structure would be necessary to understand this issue better.

The soot induction delay time for the FT was found to decrease appreciably when oxygen concentration increased. This result is similar to previous findings, for example with *n*-propylcyclohexane [16] or *n*-decane [13]. However, the amplitude of the oxygen effect on τ_{ind} depends on the structure of the initial hydrocarbon, as can be seen in [16]. This promoting effect of oxygen on τ_{ind} was explained with acetylene–oxygen mixtures in [35], where the enhancement of the fuel decomposition, leading to a sufficiently high concentrations of radicals that enhance the soot formation process, was described. The rapid formation of hydrogen atoms during the first steps of soot precursors formation was also reported and was found to enhance the polymeric growth of polycyclic aromatics. These effects of oxygen are also responsible for the shift toward lower temperatures of the soot yield curve, whereas the decrease of the soot yield is due to the oxidation of the soot particles.

Over the range of investigated concentrations, τ_{ind} was found to be relatively insensitive to the FT concentration using the classical measurement method. A promoting effect of the fuel concentration was, however, generally observed in the literature with aromatics [27,36] or unsaturated species [24] using the same measurement method. Overall, this indicates that the fuel concentration effect on the induction delay time is not very important for a mixture

of paraffins under the conditions investigated. These induction delay time results, when compared with Fig. 5, also exhibit the ambiguous signification of the induction delay time in soot extinction measurements, as mentioned by Wang [37]. Indeed, if different measurement methods (pressure profile, radical emission) or wavelengths (OH^* at 307 nm or CH^* at 431 nm) generally yield the same ignition delay time during the oxidation of hydrocarbons [38], the measurement of the soot induction delay time changes greatly with the wavelength used to follow the light extinction profile. Still, the induction delay time can be used as a guide to estimate, by comparison, the soot propensity of a fuel. To have an induction delay time that better represents the observed results from soot volume fraction profiles, it should be defined based on another criterion, such as the time between the moment at which the reflected shock wave heats up the mixture and the moment at which the soot volume fraction signal reaches an arbitrary threshold value. Figure 11 presents the determination of the induction delay time using this threshold method for two carbon concentrations and with threshold values set to 5×10^{-8} (Fig. 11a) and 1×10^{-7} (Fig. 11b). As can be seen from this figure for both threshold values, the induction delay time is shorter for the greater fuel concentration. For a threshold value of 5×10^{-8} , the induction delay time is 1170 μs for the 0.2% FT mixture and 1020 μs for 0.4% FT (Fig. 6a). If the threshold value is fixed to 1×10^{-7} , then the induction delay time is 1260 μs for the 0.2% FT mixture and 1150 μs for 0.4% FT (Fig. 5b).

Results employing this method of determination of the induction delay time are presented in Fig. 12 for the threshold value of 5×10^{-8} . It can be seen in this figure that the induction delay times at the lowest fuel concentration are now slightly longer than the delay times determined at 0.4% FT, as observed experimentally from the soot volume fraction profiles (Fig. 5). Note that it is important to select a low threshold value to measure the induction delay time. Indeed, too high a value would give the same kind of results as the classical method of determination of τ_{ind} and would tend to increase the experimental scattering. A value of $5 \times 10^{-8} \text{ cm}^3/\text{cm}^3$ was determined to be appropriate for this study. However, it is worth mentioning that this alternative method does not remove the ambiguity in the induction delay time signification. Ideally, the induction delay time would be defined by the time between the arrival of the reflected shock wave and the moment at which the single soot particles reach a given average diameter. The minimum diameter for such nuclei, to be observable is usually considered to be between 1 and 2 nm. These solid nuclei will be responsible for a certain amount of light extinction. Increasing the carbon concentration in the gaseous phase will then induce the formation of more soot nuclei (their density number should be higher) and hence a higher soot volume fraction should be observed earlier even if the chemistry is not faster, as is probably the case in this study. However, such measurement of the diameter of the nascent soot particles would be difficult to perform under our conditions and with our system. Another alternative would be to follow the time evolution of the CH^* radical and to determine an induction delay time from this measurement. However it is very likely that this measurement would correspond only to some chemical reactions in the gas phase that are taking place before the formation of the first soot particles.

With respect to Y_{max} , a strong decrease with the carbon concentration was observed, as documented in [27,36]. However, this effect is not as important as it is for toluene [27], for example. Also, while the literature generally reports a constant value [39] or an increase [36] in T_{opt} when the fuel concentration is decreased, a lower value in T_{opt} for the lowest FT concentration was observed in the present study. This decrease in T_{opt} is associated with a shift toward lower temperatures of the lowest temperature at which soot is detected. It is not immediately clear why this is, and points

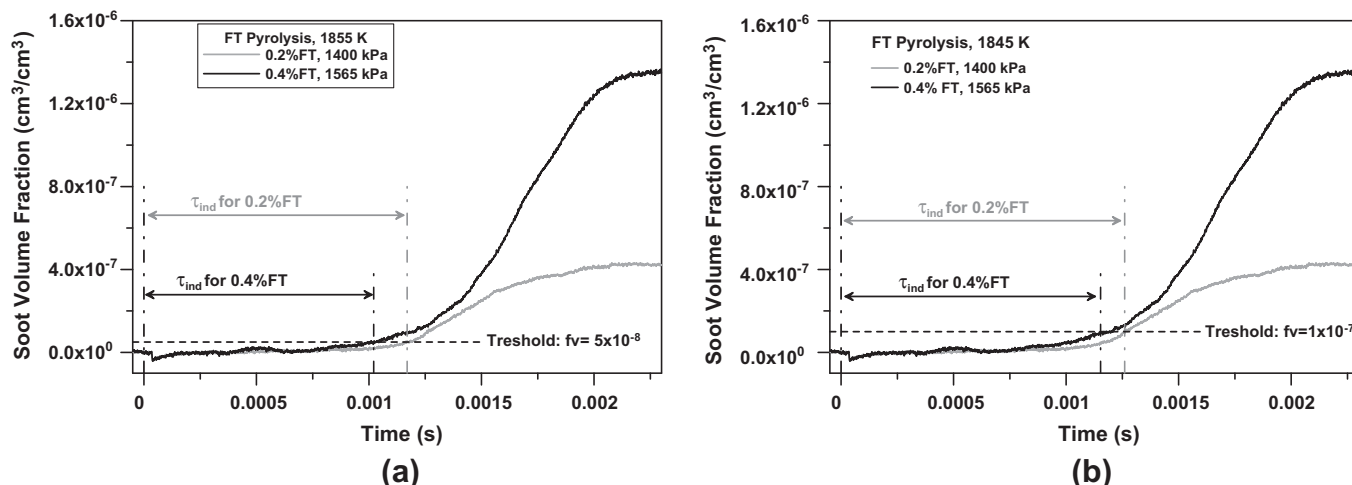


Fig. 11. Soot volume fraction versus time in the case of the pyrolysis of two different fuels molar percent at a temperature of 1855 K. (a) soot volume fraction threshold = 5×10^{-8} and (b) volume fraction threshold = 1×10^{-7} .

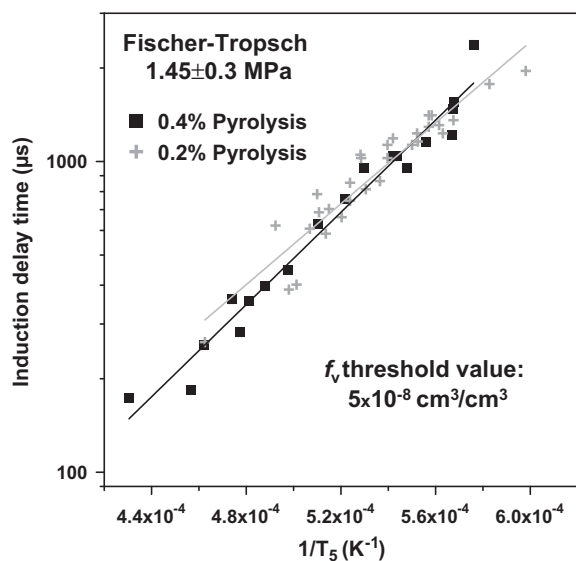


Fig. 12. Evolution of the soot induction delay with the temperature behind the RSW for the pyrolysis at around 1.45 MPa of a distillation cut at 403 K of a Fischer-Tropsch fuel. Soot induction delay time was determined using a threshold value for the soot volume fraction profile of 5×10^{-8} . Lines: best fit.

to the need for a comprehensive study of the fuel concentration effect on soot formation under shock tube environment.

In a former study, Mathieu et al. [16] derived an expression that allows determination of the maximum soot yield as oxygen is added to the mixture when the maximum soot yield that can be achieved during the pyrolysis of a given fuel is known:

$$Y_{\max, \Phi} = Y_{\max, \text{pyrolysis}} \cdot \left[1 - \left(\frac{2.5}{\Phi} \right)^{0.5} \right] \quad (3)$$

This expression (3) was successfully applied to alkylaromatics, from toluene to *n*-heptylbenzene, in [16]. The maximum soot yield using Eq. (3) for the FT at 0.4% would be 3.9% at $\Phi = 18$ and 1.8% at $\Phi = 5$ when the value determined experimentally during the pyrolysis of 0.4% FT was used. These values are very close (3.8% at $\Phi = 18$) or within fair agreement (1.4% at $\Phi = 5$) to the values derived experimentally. It can therefore be concluded that the expression (3) is also valid for alkane fuels. This result would indicate a soot reduction mechanism with O_2 that is common regardless of the structure

of the initial fuel. One can therefore conclude that the effect of O_2 on the soot yield mostly takes place at the soot level, through heterogeneous oxidation, rather than in the gas phase when the first soot precursor are formed from the parent fuels.

The comparison between the FT and the surrogate showed a large difference in τ_{ind} , which can be translated by a higher soot propensity of the diesel surrogate. Comparison between soot yields showed that mixtures of hydrocarbons can have significantly different behavior depending on their composition. In the case of the FT, composed of only one class of chemical compounds (paraffins), one peak is observed; whereas two peaks were observed for the surrogate (composed of three classes of chemical compounds: paraffin, naphthene, and aromatic) [16]. This observation marks the importance of the initial fuel composition during the soot formation process and the fact that synergistic effects can be observed within a class of compounds, which is not necessarily the case for mixtures that include several classes of hydrocarbons.

The comparison between soot yields from the FT and the diesel surrogate does not allow commenting on the higher soot propensity of the surrogate. This could be due to the fact that the FT studied is a low-temperature distillation cut of a diesel boiling range FT and Fig. 9 shows that, at a constant carbon concentration, the shorter the paraffin, the higher the soot yield; i.e. the soot yield of the FT cut is certainly higher than it would be for the complete diesel FT under similar conditions. In addition, the diesel surrogate was formulated using the compound class composition approach with polyaromatic species lumped with aromatics (represented by *n*-butylbenzene). Polyaromatics, such as 1-methylnaphthalene, exhibit an extremely high soot propensity compared to other class of compounds [14]. The fact that polyaromatics were not included in the surrogate formulation, even in modest proportions, could seriously reduce the soot propensity of the diesel surrogate when compared to a real diesel fuel. Similarly, *n*-propylcyclohexane was chosen to represent naphthenes in the surrogate. But, polycycloalkanes, such as decalin, have a higher soot propensity [14], and it probably would have been better to incorporate decalin into the surrogate formulation to better represent a real diesel fuel. In other words, the soot formation propensity of this specific FT distillation cut might have been artificially increased by the cut in the boiling curve, whereas the soot formation propensity of the diesel surrogate might have been artificially reduced, because of its formulation. As a result, the maximum soot yield is comparable between the two mixtures (even if the diesel surrogate produces soot over a wider range of temperatures in pyrolysis). At $\Phi = 5$,

surprisingly, the FT distillation cut produces more soot than the diesel surrogate. To date, there are no clear explanations that help understand this result, but it may be due to differences between soot structures and their resistance to oxidation. Indeed, Vander Wal and Tomaseck [40,41] showed that, at high temperature and for a low residence time, the nature of the initial hydrocarbon has a strong influence on the structure of the soot [40], and that the soot structure is a key parameter for the soot oxidation process [41]. A systematic TEM study of the soot structure for these two fuels would, however, be necessary to clarify the results observed in this study at $\Phi = 0.5$.

6. Conclusions

During this study, the soot formation process from a distillation cut at 403 K of a diesel Fischer–Tropsch fuel was investigated in a heated shock tube. Results showed the appearance of a second growth stage of the soot volume fraction for the highest fuel concentration investigated, in pyrolysis and at $\Phi = 18$. This second growth was found to be sensitive to carbon and oxygen concentrations and temperature. These observations support the chemical origin theory of this phenomenon postulated in [16].

The measurement of the soot induction delay time is discussed and two different methods are compared. Although the standard method usually adopted in the literature is probably not ideal, it is still useful for a systematic comparison or when large differences in the soot tendency exist.

If the FT concentration does not have a strong influence on τ_{ind} , a strong effect of oxygen on the induction delay time is, however, observed. The oxygen enhances the soot formation process (reduction of the τ_{ind} , shift of the soot yield curves toward lower temperatures) but reduces, through heterogeneous oxidation, the amount of soot generated and, therefore, the soot yield. Comparison with literature data showed that the FT distillation cut, which is mainly composed of *n*-paraffins, can be relatively well represented by *n*-decane, on *n*-paraffin whose molecular size is somewhat comparable to the average molecular size of the FT distillation cut. This finding, if transposable, makes some FT fuels very interesting for numerical investigations using a single paraffin. Comparison with a diesel surrogate does not show a significant difference from the FT in terms of soot yield reduction ability. This result is probably due to the surrogate formulation and to the fact that only a light cut of the FT diesel fuel was studied. Nevertheless, it is worth mentioning that these results are interesting for jet fuel studies, as the FT distillation cut would correspond to the boiling range of a jet fuel.

Acknowledgment

The authors thank Total for financial support of this study under contract CNRS-TOTAL N° 081.1564.0.

References

- [1] I.M. Kennedy, Proc. Combust. Inst. 31 (2007) 2757–2770.
- [2] D. Leckel, Energy Fuels 23 (2009) 2342–2358.

- [3] A.P. Steynberg, H.G. Nel, Fuel 83 (2004) 765–770.
- [4] R.W.R. Zwart, H. Boerrigter, Energy Fuels 19 (2005) 591–597.
- [5] T.L. Alleman, R.L. McCormick, SAE Paper No. 2003-01-0763, 2003.
- [6] A. Abu-Jrai, A. Tsolakis, K. Theinnoi, R. Cracknell, A. Megaritis, M.L. Wyszynski, S.E. Golunski, Energy Fuels 20 (2006) 2377–2384.
- [7] M.S.P. Kahandawala, J.L. Graham, S.S. Sidhu, Energy Fuels 18 (2004) 289–295.
- [8] S.M. Hwang, P. Vlasov, H. Gg. Wagner, Th. Wolff, Z. Phys. Chem. 173 (1991) 129–139.
- [9] M. Evans, A. Williams, Fuel 60 (1981) 1047–1056.
- [10] H. Kellerer, A. Muller, H.-J. Bauer, S. Wittig, Combust. Sci. Technol. 113–114 (1996) 67–80.
- [11] H. Kellerer, R. Koch, S. Wittig, Combust. Flame 120 (2000) 188–199.
- [12] Z. Hong, D.F. Davidson, S.S. Vasu, R.K. Hanson, Fuel 88 (2009) 1901–1906.
- [13] D. Darius, N. Chaumeix, C. Paillard, Pyrolysis and oxidation of *n*-decane, *n*-propyl-benzene and kerosene surrogate behind reflected shock waves, in: Int. Workshop on Combustion Generated Fine Carbon Particles, Villa Orlandi, Italy, May 13–16, 2007.
- [14] F. Douce, N. Djebaïli-Chaumeix, C.-E. Paillard, C. Clinard, J.-N. Rouzaud, Proc. Combust. Inst. 28 (2000) 2523–2529.
- [15] N. Djebaïli-Chaumeix, D. Ladril, C.-E. Paillard, in: G.D. Roy, S.M. Frolov, A.M. Starik (Eds.), Combustion and Atmospheric Pollution, Torus Press Ltd., 2003, pp. 411–417.
- [16] O. Mathieu, N. Djebaïli-Chaumeix, C.-E. Paillard, F. Douce, Combust. Flame 156 (2009) 1576–1586.
- [17] W.C. Gardiner Jr., B.F. Walker, C.B. Wakefield, in: A. Lifshitz (Ed.), Shock Waves in Chemistry, Dekker, New York, 1981, pp. 319–374.
- [18] S.H. Bauer, L.M. Zhang, in: Proc. of the 14th Int. Symposium of Shock Tube and Waves, Sydney, Australia, 1983.
- [19] S.C. Lee, C.L. Tien, Proc. Combust. Inst. 18 (1981) 1159–1166.
- [20] T.C. Williams, C.R. Shaddix, K.A. Jensen, J.M. Suo-Anttila, Int. J. Heat Transfer 50 (2007) 1616–1630.
- [21] A. Burcat, B. Ruscic, Third Millennium Ideal Gas and Condensed Phase Thermochemical Database for Combustion with updates from Active Thermochemical Tables, ANL-05/20 and TAE 960 Technion-IT, Aerospace Engineering, and Argonne National Laboratory, Chemistry Division, September 2005.
- [22] E.R. Ritter, J.W. Bozzelli, THERM: Thermodynamic Property Estimation for Radicals and Molecules, User's Manual, New Jersey Institute of Technology, Newark, NJ, March 16, 1987.
- [23] S.W. Benson, Thermochemical Kinetics, second ed., Wiley, New York, 1976.
- [24] M. Frenklach, S. Taki, M.B. Durgaprasad, R.A. Matula, Combust. Flame 54 (1983) 81–101.
- [25] M. Frenklach, T. Yuan, M.K. Ramachandra, Energy Fuels 2 (1988) 462–480.
- [26] S.C. Graham, J.B. Homer, J.L.J. Rosenfeld, Proc. R. Soc. London, A 344 (1975) 259–285.
- [27] O. Mathieu, G. Frache, N. Djebaïli-Chaumeix, C.-E. Paillard, G. Krier, J.-F. Muller, F. Douce, P. Manuelli, Proc. Combust. Inst. 31 (2007) 511–519.
- [28] Y. Takatori, Y. Mandokoro, K. Akihama, K. Nakakita, Y. Tsukasaki, S. Iguchi, L.I. Yeh, A.M. Dean, SAE Paper 982495, 1998, pp. 1181–1187.
- [29] M.L. Huber, B.L. Smith, L.S. Ott, T.J. Bruno, Energy Fuels 22 (2008) 1104–1114.
- [30] B.L. Smith, T.J. Bruno, J. Propuls. Power 24 (2008) 618–623.
- [31] M.S.P. Kahandawala, M.J. DeWitt, E. Corporan, S.S. Sidhu, Energy Fuels 22 (2008) 3673–3679.
- [32] A. Emelianov, A. Eremin, E. Gurentsov, A. Makeich, H. Jander, H. Gg. Wagner, P. Roth, R. Starke, Proc. Combust. Inst. 30 (2005) 1433–1440.
- [33] M. Frenklach, J.P. Hsu, D.L. Miller, R.A. Matula, Combust. Flame 64 (1986) 141–155.
- [34] G.L. Agafonov, V.N. Smirnov, P.A. Vlasov, Effect of iron pentacarbonyl on soot formation behind shock waves, in: Proceedings of the 23rd ICDEERS, Irvine, CA, USA, July 24–29, 2011.
- [35] M. Frenklach, D.W. Clary, T. Yuan, W.C. Gardiner Jr., S.E. Stein, Combust. Sci. Technol. 50 (1986) 79–115.
- [36] A. Alexiou, A. Williams, Combust. Flame 104 (1996) 51–65.
- [37] H. Wang, in: G. Ben-Dor, O. Igara, T. Elperin (Eds.), Handbook of Shock Waves, vol. 3, Academic Press, 2001, pp. 257–308 (Chapter 16.6).
- [38] B.M. Gauthier, D.F. Davidson, R.K. Hanson, Combust. Flame 139 (2004) 300–311.
- [39] S.T. Bauerle, Y. Karasevich, S.T. Slavov, D. Tanke, M. Tappe, T.H. Thienel, H. Gg. Wagner, Proc. Combust. Inst. 25 (1994) 627–634.
- [40] R.L. Vander Wal, A.J. Tomaseck, Combust. Flame 136 (2004) 129–140.
- [41] R.L. Vander Wal, A.J. Tomaseck, Combust. Flame 134 (2003) 1–9.